J Mater Sci (2012) 47:3729–3740
DOI 10.1007/s10853-011-6222-0

Ferroelectric phases and relaxor states in the novel lead-free $(1 - x)$ $Bi_{1/2}K_{1/2}TiO_3 - x$ $BiScO_3$ system $(0 \leq x \leq 0.3)$

L. Martín-Arias · A. Castro · M. Algueró

Received: 4 October 2011 / Accepted: 20 December 2011 / Published online: 7 January 2012

Abstract The novel lead-free Bi-based ferroelectric system with perovskite structure $(1 - x)$ $Bi_{1/2}K_{1/2}TiO_3 - x$ $BiScO_3$, chemically designed to show a ferroelectric morphotropic phase boundary (MPB) and high piezoelectric response, was synthesized by the conventional solid-state reaction method for compositions with $0 \leq x \leq 0.3$. X-ray diffraction analysis shows that the samples possess perovskite-type structure for $x < 0.3$ and reveals a phase evolution in the symmetry from tetragonal for $x < 0.1$ to pseudocubic for $0.1 \leq x \leq 0.3$. Electrical and piezoelectric properties of ceramic samples were systematically investigated, and results indicate that a ferroelectric MPB is not formed, but instead a transition from conventional ferroelectric to relaxor ferroelectric behavior occurs when increasing the (Bi, Sc) content between 5 and 10%. The origin of this unexpected effect, and its implications in the design of novel lead-free piezoelectric materials are discussed.

Introduction

Environmental pollution is one of the main causes of concern nowadays, which has led to harsh environmental regulations being taken. In the case of piezoceramics, they require the search for lead-free materials with comparable properties to those of the well-known lead-based ferroelectric perovskites like $Pb(Zr,Ti)O_3$ (PZT) [1]. In PZT ceramics with composition lying near the morphotropic phase boundary (MPB) between the tetragonal and rhombohedral phases, high dielectric and piezoelectric properties are found. This is due to the presence of a monoclinic C*m* phase at the MPB, which provides a path for the polarization to rotate between its directions in the rhombohedral and tetragonal phases, and has associated an enhanced electromechanical response [2]. Several solid solutions have been targeted in the quest for lead-free or lead-less substitutes for PZT, which were designed to obtain analogous MPBs and equally high piezoelectric properties [3–6].

$K_{1-x}Na_xNbO_3$ is one such system that has been thoroughly investigated during the last years because of its high Curie temperature T_C and good piezoelectric properties [7]. High values of piezoelectric coefficients, comparable to those of PZT, are obtained by the downward shift of the temperature of the orthorhombic to tetragonal phase transition T_{O-T}, by doping. High coercive field and low remnant polarization, with some exceptions, and their difficult processing are, however, cause of concern. Yet their main problem is the temperature dependence of their properties and degradation caused by thermal cycling between the different ferroelectric states. This is a common problem for materials that have been engineered to be at polymorphic phase transitions, those for which the phase transition is controlled with temperature, so materials with MPBs, which involve a phase evolution with composition, are thus preferred. Examples of actual MPB systems are $BiScO_3$–$BaTiO_3$ [8, 9] and the widely studied $Bi_{1/2}Na_{1/2}TiO_3$–$BaTiO_3$ [10], for which enhanced properties have been reported. However, in the latter case, T_C shifts to lower temperatures with $BaTiO_3$ addition as compared with that of the Bi-containing perovskite. Also, there is a ferro–antiferroelectric transition that occurs at temperatures much lower than T_C, which further decreases the operation temperature range. Therefore, a suitable candidate to replace PZT has not been found yet.

L. Martín-Arias · A. Castro · M. Algueró (✉)
Instituto de Ciencia de Materiales de Madrid, CSIC,
Cantoblanco, 28049 Madrid, Spain
e-mail: malguero@icmm.csic.es

A lead-less material with interesting properties is $BiScO_3$–$PbTiO_3$ [11]. The $BiScO_3$–$PbTiO_3$ (BS–PT) system exhibits better performance than PZT near the MPB, at 64 mol% PT, between rhombohedral and tetragonal phases. It has a considerably higher T_C (450 °C) than that of PZT, a wider range of thermal stability [12], and a competitive value of piezoelectric coefficient d_{33} (450 pC/N), which demonstrates the important role played by the BS content in enhancing T_C while maintaining high piezoelectric coefficients [13]. The MPB region of $BiScO_3$–$PbTiO_3$ is analogous to that of PZT, exhibiting a monoclinic C*m* phase between the rhombohedral and tetragonal polymorphs [14, 15].

Based on $BiScO_3$–$PbTiO_3$ as a good precedent of a lead-less system with a MPB, we have studied the $(1-x)$ $Bi_{1/2}K_{1/2}TiO_3 - x$ $BiScO_3$ (BKT–BS) solid solution as a lead-free alternative. $Bi_{1/2}K_{1/2}TiO_3$ (BKT) was chosen because: (1) it crystallizes in a tetragonal symmetry, so it can potentially form a rhombohedral tetragonal MPB; and (2) Bi^{3+} has a high polarizability and a lone pair, which has been suggested to be essential to maintain good ferro and piezoelectric properties [16].

Experimental procedures

Submicron or micrometric sized powders of $(1-x)$ $Bi_{1/2}K_{1/2}TiO_3 - x$ $BiScO_3$ with $0 \leq x \leq 0.3$ were prepared by the traditional solid-state reaction method, using Bi_2O_3 (Sigma-Aldrich, 99.9%, particle size < 10 μm), TiO_2 (Sigma-Aldrich, +99.9%, particle size < 5 μm), Sc_2O_3 (Sigma-Aldrich, 99.9%, powder), and K_2CO_3 (Sigma-Aldrich, 99.995%, powder) as starting materials. The initial products were weighted according to the stoichiometric composition and then thoroughly mixed by hand in an agate mortar. Prior to weighing, the K_2CO_3 powder was dried at 150 °C for 24 h in a stove, to remove any water content, and cooled to room temperature in a desiccator.

This method requires cumulative treatments for the perovskite phase to be obtained. The heating sequence followed in this study was 12 h at 500, 600, 700, 800, 850, 900, 950, 960, 975, 985, and 1000 °C. Hand homogenization and characterization by X-ray powder diffraction (XRD) at room temperature were carried out after each consecutive step to establish the best conditions for synthesizing the different phases. Thermal treatments were interrupted before phase decomposition and the formation of secondary phases was observed. Phases and crystal structure were studied by XRD, with a Bruker AXD D8 Advance diffractometer using the Cu K_α doublet ($\lambda = 0.15418$ nm). The patterns were recorded between 12° and 60° (2θ), with increments of 0.05° (2θ) and a counting time of 1.5 s/step. Cell parameters were calculated from XRD data by means of a least squares refinement method (CELREF).

The morphology of the synthesized powders was examined by field emission scanning electron microscopy (FE-SEM) with a FEI Nova NanoSEM 230 scanning electron microscope operating between 3 and 10 kV, equipped with an Oxford INCA 250 energy dispersive X-ray spectrometer (EDXS).

The calcined powders were uniaxially pressed into 12 mm diameter and 1.2 mm thick disks. The green pellets were sintered at 950–1000 °C for 2 h in air. Synthesis temperatures proved to be adequate as sintering temperatures in all cases. The density of the ceramics was obtained by the Archimedes method with distilled water. Microstructure was studied in fracture surfaces with the same FE-SEM apparatus.

The thickness of the resulting ceramic disks was reduced down to 0.5 mm by means of polishing. Silver paste was painted on both sides of the samples and annealed at 700 °C, as electrodes for the subsequent electric measurements. The temperature dependence of the dielectric permittivity at nine frequencies, between 100 Hz and 1 MHz, was measured with an HP4284A precision LCR-meter during a heating/cooling cycle, between room temperature and 500 °C, at a 1.5 °C/min rate. Low frequency (0.1 Hz) voltage sine waves with amplitudes up to 5 kV were applied for the characterization of the nonlinear electric response at room temperature by the combination of a synthesizer/function generator (HP 3325B) and a TREK MODEL 10140 high voltage amplifier. Charge was measured with a homebuilt charge-to-voltage converter and software for loop acquisition and analysis.

The samples were poled for their piezoelectric characterization. The high coercive field and the non-negligible conductivity of the $(1-x)$ BKT $- x$ BS ceramics rendered the poling difficult. First, the samples were poled at successively higher values of the poling field until dielectric breakdown occurred. Second, a milder poling was performed by increasing the temperature up to successively higher values, maintaining the samples under a 5 kV/mm electric field for 5 min at each maximum temperature, and keeping the field on during cooling down to room temperature. The longitudinal piezoelectric coefficient d_{33} achieved under the different poling conditions was measured with a Berlincourt type meter 24 h after the poling steps.

Results and discussion

Powdered samples

Synthesis

Solid solutions of $(1-x)$ BKT $- x$ BS with x ranging from 0 to 0.3 were investigated. The XRD patterns of the

different compositions at different stages of the synthesis and at the end of the synthesis are shown underneath. Figure 1 shows the effect of successive thermal treatments at increasing temperatures on the synthesis of the $(1 - x)$ $Bi_{1/2}K_{1/2}TiO_3 - x$ $BiScO_3$ solid solution with: (a) $x = 0$ and (b) $x = 0.3$. The black circles indicate the presence of $Bi_{12}TiO_{20}$ (JCPDS 340097) as an intermediate phase after treatment at 600 °C. This feature was observed in the XRD patterns of all investigated compositions. This phase disappears after subsequent treatment at 700 °C for the compositions with $x = 0$. Successively higher temperatures are required for its disappearance as the bismuth and scandium content is increased, up to the point where it can no longer be totally eliminated through successive calcination for $x = 0.3$. Besides, traces of other secondary phases are detected in the final sample with $x = 0.3$ at 950 °C, which amount increases with further heating. $Bi_4Ti_3O_{12}$ (JCPDS 120213) is commonly encountered as intermediate phase in the synthesis of most of bismuth perovskites. This might be the case for the $x = 0.3$ composition. Nonetheless, overlapping of the main peaks in the diffraction data hinders an utter identification of the secondary phases.

With regard to the optimum synthesis temperatures of the different $(1 - x)$ BKT $- x$ BS compositions two distinct behaviors can be observed as bismuth and scandium are introduced. First, an increasing temperature is required to complete the synthesis, which results in larger final crystallinity as revealed by the narrowing of the peaks in the XRD data. However, for solid solutions with larger substituting elements content ($x > 0.1$) the synthesis temperature needs to be lowered in order to prevent phase decomposition.

Figure 2 shows XRD patterns of the final $(1 - x)$ BKT $- x$ BS calcined powders as a function of bismuth and scandium contents, at room temperature. Perovskite single phases were obtained for $x < 0.3$ and the crystalline structure of the compounds evolves from tetragonal for $x < 0.1$ to pseudocubic for $0.1 \leq x \leq 0.3$.

It is evident that a small amount of both substituting elements ($x = 0.05$) diminishes the tetragonality of BKT. In fact, further addition results in a phase transition toward a pseudocubic symmetry that appears for $x = 0.1$, and remains with increasing bismuth and scandium concentration up to the composition with the highest content studied ($x = 0.3$). Yet it should be noted that the composition with $x = 0.3$ cannot be regarded as pure perovskite phase of pseudocubic symmetry due to the presence of secondary phases, as previously commented. The phase transition can be clearly seen in Fig. 2 from the merging of the tetragonal

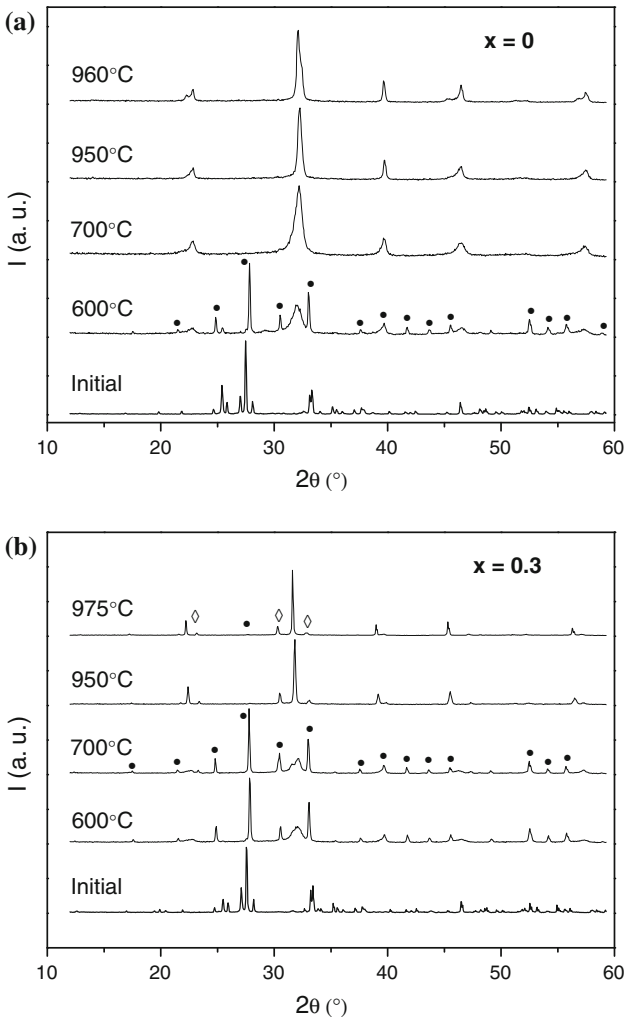

Fig. 1 XRD patterns of the $(1 - x)$ $Bi_{1/2}K_{1/2}TiO_3 - x$ $BiScO_3$ powders with: **a** $x = 0$ and **b** $x = 0.3$ at different stages of the synthesis (*filled circle* $Bi_{12}TiO_{20}$, *open diamond* secondary phases)

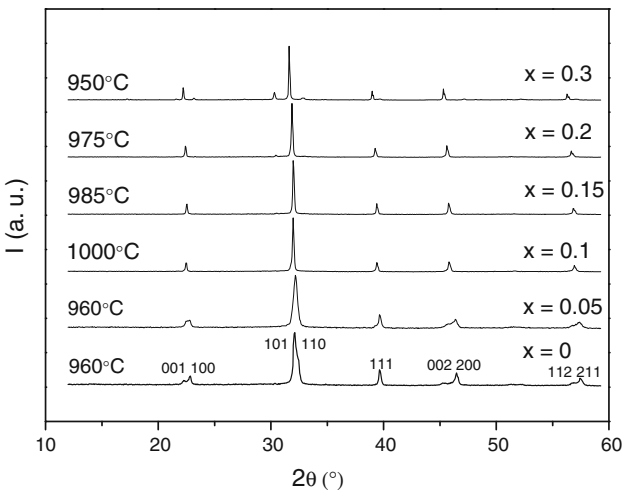

Fig. 2 XRD patterns of the $(1 - x)$ $Bi_{1/2}K_{1/2}TiO_3 - x$ $BiScO_3$ powders of the final phases for all studied compositions. Tetragonal $Bi_{1/2}K_{1/2}TiO_3$ perovskite is indexed

doublets (001)(100), (002)(200), and (112)(211) into the corresponding pseudocubic singlets.

Crystal structure characterization In order to gather more detailed crystallographic information concerning structural changes as a consequence of substitution, the unit-cell parameters were determined. Least square refinements were performed on the XRD data for the different compositions. The phases corresponding to the compositions with $x = 0$ and $x = 0.05$ were refined with a perovskite tetragonal phase (space group *P4mm*, No. 99) from the starting model of undoped BKT. Compositions with $0.1 \leq x \leq 0.3$ were refined assuming a cubic structure with a centro-symmetric space group $P\ \bar{m}3m$ (No. 221). The lattice parameters obtained from the refinements and the unit-cell volume of the $(1 - x)$ BKT $- x$ BS powders as a function of composition are shown in Figs. 3 and 4, respectively. The tetragonal distortion *c/a* is reduced with increasing bismuth and scandium substitution as a combined effect of decrease in *c* and increase in *a* lattice parameters, until vanishing for $x = 0.1$. A cell expansion is observed when the amount of bismuth and scandium is increased from $x = 0.05$ to $x = 0.1$, coinciding with the phase transition from tetragonal to pseudocubic. On the other hand, little volume variation happens with further increase of both cations once the phase transition occurs ($x > 0.1$).

A tetragonal to pseudocubic phase transition was also reported in the system $(1 - x)\ Na_{1/2}K_{1/2}NbO_3 - x\ BiScO_3$ upon increasing the bismuth and scandium content further than a 2% [17] Also, Datta et al. [18] recently reported an analogous change in the crystalline structure from tetragonal to pseudocubic for the $(1 - x)\ BaTiO_3 - x\ BiScO_3$ system. The latter authors propose this phase transition to be a consequence of the induced microstrain upon doping,

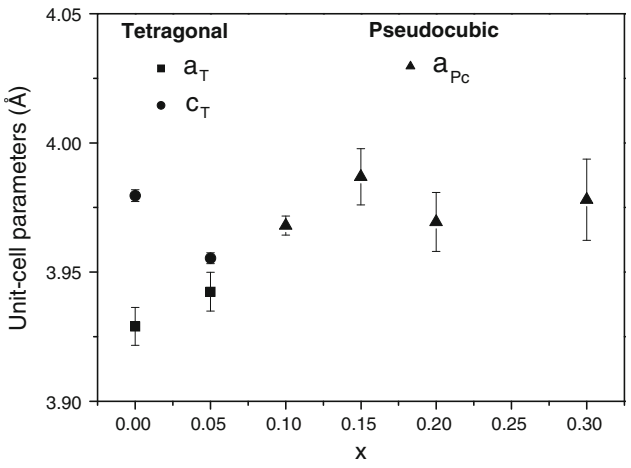

Fig. 3 Unit-cell parameters for the $(1 - x)\ Bi_{1/2}K_{1/2}TiO_3 - x\ BiScO_3$ ceramics as a function of composition, showing the evolution from the tetragonal to the pseudocubic phase

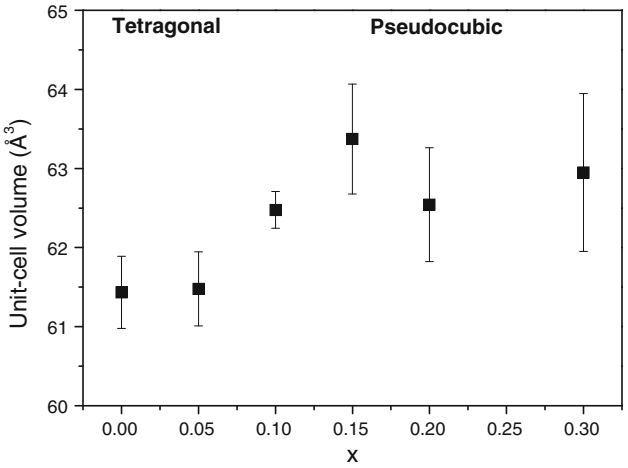

Fig. 4 Unit-cell volume of the $(1 - x)\ Bi_{1/2}K_{1/2}TiO_3 - x\ BiScO_3$ perovskites as a function of composition

based on a previous theoretical study that showed the inhibition of the cubic to tetragonal transition in $BaTiO_3$ by strain [19]. Nevertheless, we will show later that this seems not to be the case for $(1 - x)\ Bi_{1/2}K_{1/2}TiO_3 - x\ BiScO_3$.

Morphology

In relation to powder morphology, Fig. 5 shows the SEM micrographs of the $(1 - x)$ BKT $- x$ BS powders with $x = 0$, $x = 0.1$, and $x = 0.3$. Well-defined cubic crystals of sizes ranging from 40 to 270 nm were obtained for $x = 0$. Larger perfectly cubic crystals of sizes in the range of 0.2–1 μm and a greater uniformity in morphology can be observed throughout the sample with $x = 0.1$. This is most probably rather a consequence of the higher temperature required for the synthesis than of the bismuth and scandium addition.

On the other hand, high levels of doping lead to an obvious change in the particle shape and size, as seen in the sample with the greatest *x* value ($x = 0.3$), characterized by irregular-shaped micrometric (1–2 μm) particles. Particles with significant deviations from the nominal composition of the perovskite phase were identified by EDXS, which must correspond with second phases detected by XRD. This is illustrated in Fig. 6, where the EDX spectrum of one such particle is compared with an average (over powder) spectrum. Note the Sc absence and Bi deficiency of the particle, which confirms incomplete reaction for powder with $x = 0.3$.

Ceramic materials

Processing

Dense ceramics (>94% of theoretical density) were obtained from the powders by conventional sintering at

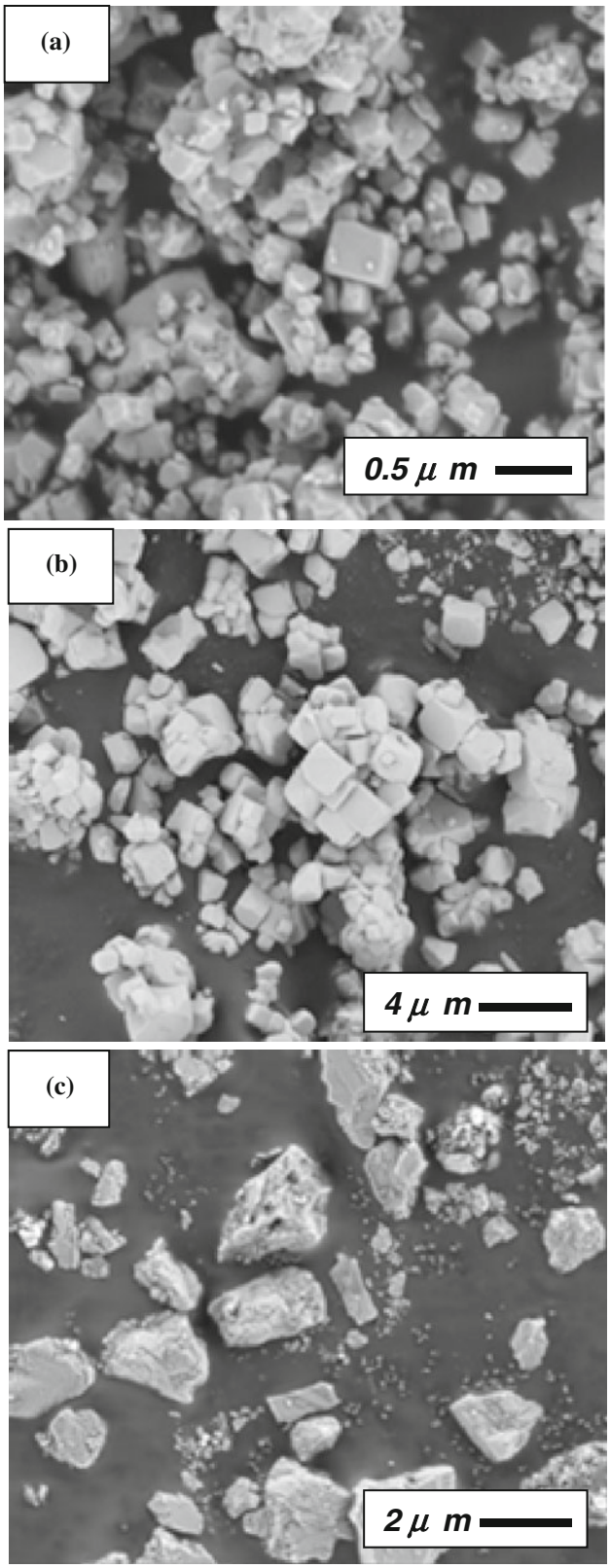

Fig. 5 Scanning electron micrographs of the $(1 - x)$ $Bi_{1/2}K_{1/2}TiO_3 - x$ $BiScO_3$ powders: **a** $x = 0$ synthesized at 960 °C, **b** $x = 0.1$ synthesized at 1000 °C, and **c** $x = 0.3$ synthesized at 950 °C

950–1000 °C for 2 h, for all the studied compositions. Sintering temperatures were those used in the synthesis. The densification and sintering temperature of the different compositions are shown in Table 1. It is clear that the small differences in densification are a consequence of the different sintering temperatures used.

There are no large differences in microstructure among the different ceramic materials. Fracture surfaces for $(1 - x)$ BKT – x BS ceramics with $x = 0.05$, $x = 0.1$, and $x = 0.3$ are shown in Fig. 7. Note that micron-size grain sizes (1–3 μm) resulted in all cases with small differences that correlate with the sintering temperature.

No secondary phases were detected by XRD in the $Bi_{1/2}K_{1/2}TiO_3$ ceramics. This confers a significant advantage to our material as compared to others reported in the literature. Some papers report a $K_2Ti_6O_{13}$ secondary phase [20], while others give account of $K_4Ti_3O_8$ [21–25], suggesting the volatilization of Bi and K as a possible factor in their formation, which is also believed to be the main reason for the poor sinterability of $Bi_{1/2}K_{1/2}TiO_3$ ceramics [24–26]. Research on chemical methods, such as sol–gel [22–24], molten salt [26], and hydrothermal synthesis [22, 24], aimed at obtaining fine and homogeneous powders with better sintering behavior, though they often require the utilization of toxic solvents, and the narrow sintering temperature range and the formation of secondary phases are still a matter of concern. On the other hand, this study reports the fabrication of single phase dense ceramics of $Bi_{1/2}K_{1/2}TiO_3$ using a conventional process. The results obtained for $Bi_{1/2}K_{1/2}TiO_3$ favorably compare with those reported by other authors on the subject. It would appear that the nanometric and submicrometric size of the powdered phases might have facilitated the sintering process, allowing it to take place at lower temperatures. Moreover, it should be mentioned that not only for $Bi_{1/2}K_{1/2}TiO_3$ but also for all the other $(1 - x)$ $Bi_{1/2}K_{1/2}TiO_3 - x$ $BiScO_3$ phases studied, the sintering temperatures were never above 1000 °C.

Dielectric properties

Dielectric properties of the dense $(1 - x)$ BKT $- x$ BS ceramics were investigated in the temperature range from room temperature up to 500 °C. The temperature dependence of the real dielectric permittivity of the different compositions studied, measured at several frequencies is shown in Fig. 8. Temperature dependence of the imaginary dielectric permittivity at the same frequencies is shown as an inset for each composition. The graphs shown are those corresponding to the heating step, though no significant differences were found between heating and cooling. Low temperature dispersion caused by conduction phenomena

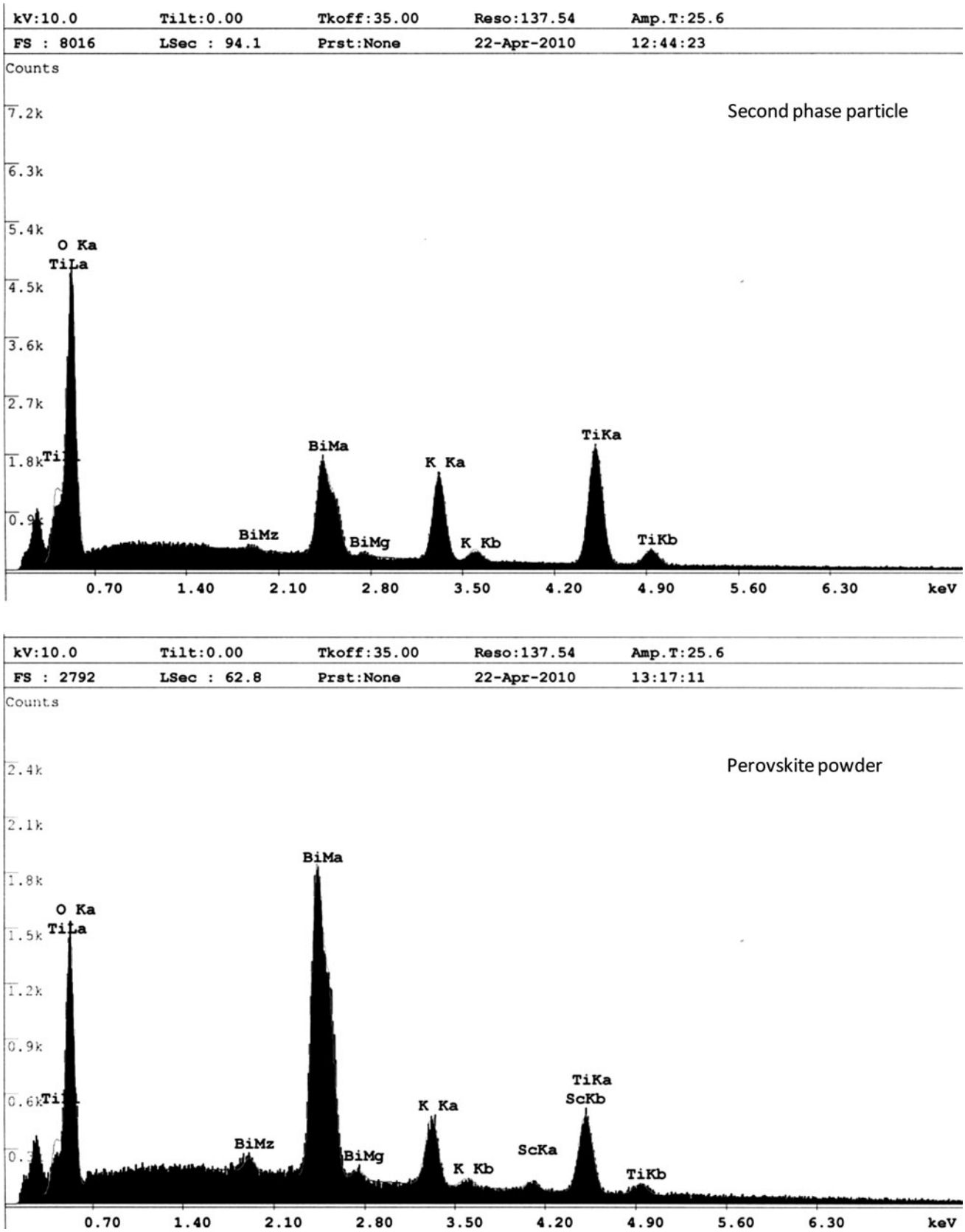

Fig. 6 EDXS spectra of the $(1 - x)\ Bi_{1/2}K_{1/2}TiO_3 - x\ BiScO_3$ powder with $x = 0.3$, and of a second phase particle

Table 1 Sintering temperature and densification of the $(1 - x)$ $Bi_{1/2}K_{1/2}TiO_3 - x$ $BiScO_3$ ceramics for the different compositions investigated

Composition (x)	Densification (%)	Sintering temperature (°C)
0	94.9	960
0.05	95.3	960
0.1	97.0	1000
0.15	95.1	985
0.2	95.6	975
0.3	94.2	950

and that disappears at 100 °C is believed to be associated to the absorption of H_2O. High temperature conductivity is also observed, most probably related to the presence of defects in the perovskite. These are most probably oxygen, bismuth and/or potassium vacancies associated with some limited (second phases are not observed) Bi_2O_3 and/or K_2O volatilization. This type of defects gives place to ionic (by oxygen vacancies electromigration) and electronic contributions to conductivity.

The compositions under study can be clearly divided into two different groups according to their electrical behavior. The first group would include the phases with $x = 0$ and $x = 0.05$. From the examination of the graphs corresponding to those compositions, it can be observed that the position and value of the permittivity maximum are not frequency dependent, especially if we focus on the high frequency graphs (100 kHz and 1 MHz), on which the dispersion due to conduction phenomena is much lower. This becomes even more obvious in the graphs of the imaginary dielectric permittivity, onto which the conductivity input appears divided by frequency. Therefore, it can be concluded that the compositions $x = 0$ and $x = 0.05$ are conventional ferroelectrics with well-defined dielectric anomalies at the temperatures of the ferroelectric transition. Note that we use the term conventional ferroelectric as opposed to relaxor ferroelectric. This means a material that shows a direct (conventional) ferroelectric transition from a paraelectric phase without intermediate relaxor states, and includes model ferroelectrics with very sharp dielectric anomalies and also ferroelectrics with diffuse phase transitions as it is the case here. Diffuseness can be caused by chemical heterogeneity, defects, microstrain, but it is a physical phenomenon different to relaxors. This is worth remarking because relaxor behavior has indeed been reported for $Bi_{1/2}K_{1/2}TiO_3$ by Yang et al. [26]. The main difference between these samples and ceramics here processed is that in our study we achieved sintering at a 100 °C lower temperature, so volatilization of Bi and K was minimized, and a smaller concentration of defects most probably results.

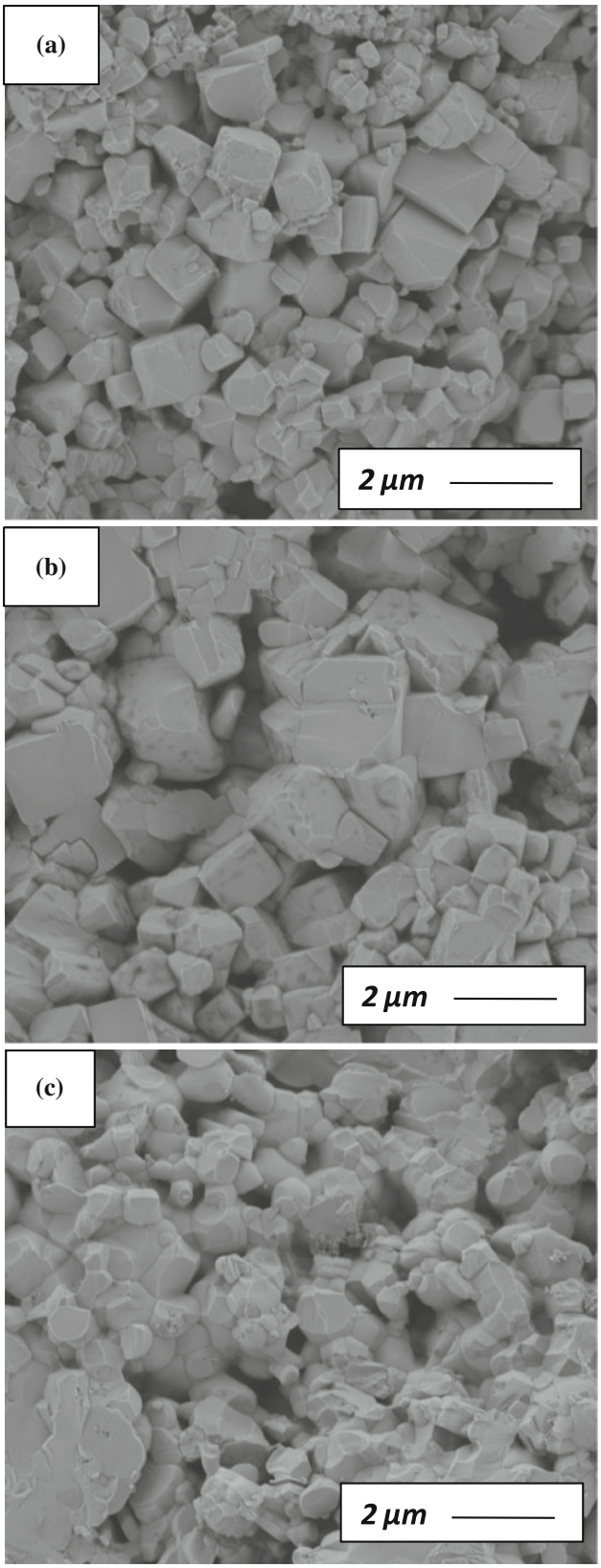

Fig. 7 Scanning electron micrographs of fracture surfaces of the $(1 - x)$ $Bi_{1/2}K_{1/2}TiO_3 - x$ $BiScO_3$ ceramics: **a** $x = 0.05$, **b** $x = 0.1$, and **c** $x = 0.3$

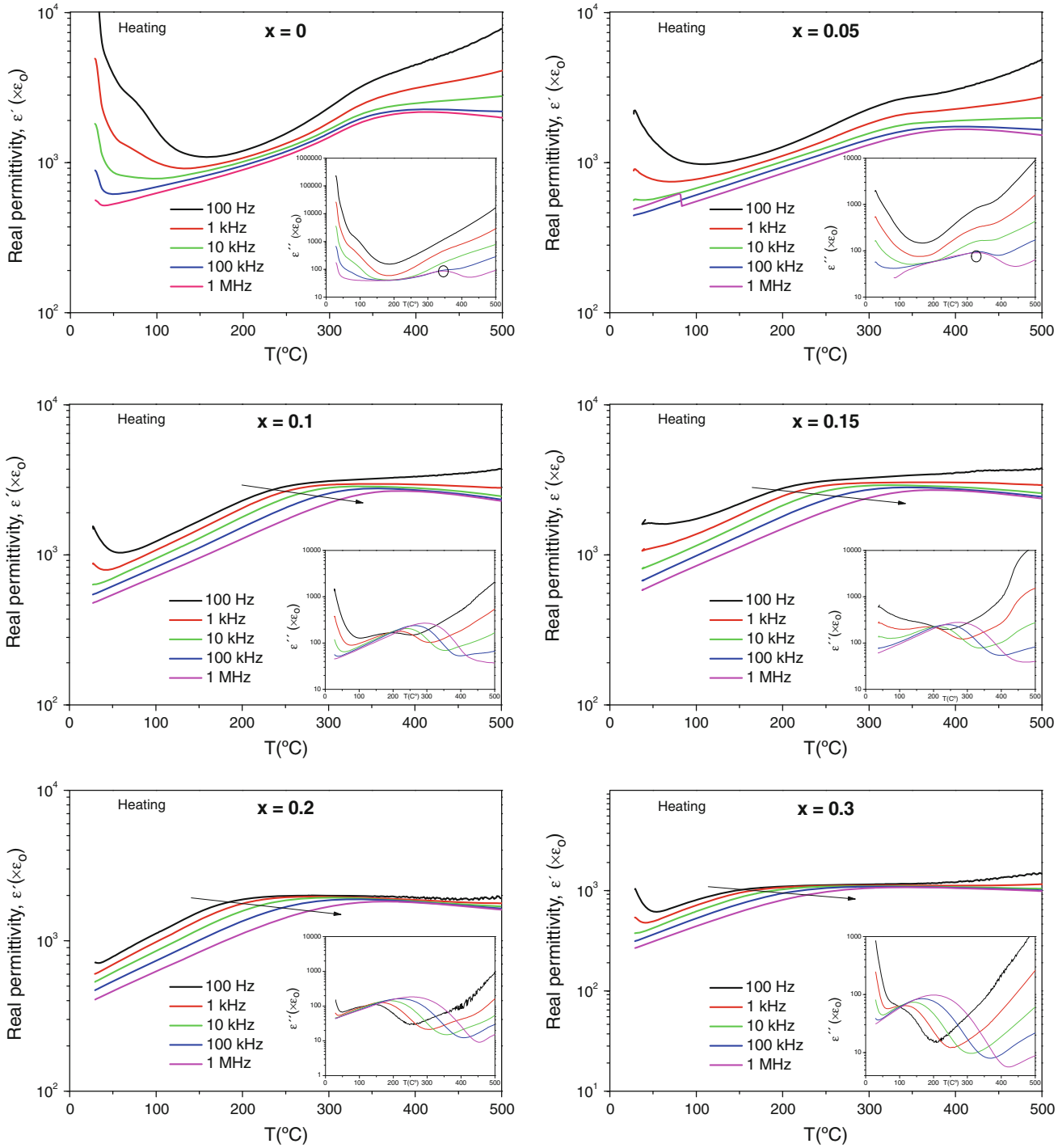

Fig. 8 Temperature dependence of permittivity on heating at several frequencies for all studied $(1 - x)\ Bi_{1/2}K_{1/2}TiO_3 - x\ BiScO_3$ compositions (imaginary parts are presented as *insets*)

The second group would comprise the compositions with $0.1 \leq x \leq 0.3$. The plots of these compositions show different features to those of the first group. Strong frequency dispersion of the maximum, which appears at higher temperatures as frequency rises, is observed in both graphs of the real and imaginary parts of dielectric permittivity. Also, whereas the real dielectric permittivity decreases when frequency increases for all temperatures, the imaginary dielectric permittivity increases with frequency in a wide temperature range around the maximum while decreasing with frequency at temperatures far from it. These results enable us to affirm that the compositions

with $0.1 \leq x \leq 0.3$ show typical relaxor behavior [27]. It must be noted that higher sintering temperatures were used in these cases.

The evolution of the temperature dependence of the real permittivity as a function of bismuth and scandium content is shown in Fig. 9a, demonstrating the effects of Bi and Sc doping on the dielectric properties of the $(1 - x)$ BKT $- x$ BS phases. The addition of a small amount ($\leq$5%) of both cations could cause an increase of chemical inhomogeneity that brings about further depletion and broadening of the dielectric maximum associated with the transition, i.e., and increase of its diffuseness. However, further increase in these cations (>5%) results in a significant increase in permittivity as the transition to a relaxor state takes place (from $x = 0.05$ to $x = 0.1$). High values of real dielectric permittivity, characteristic of relaxors are maintained with increased doping up to $x = 0.15$. Larger substitution is followed by a decrease in permittivity as a possible consequence of the quality degradation of the ceramics. The evolution of the temperature dependence of the imaginary part of the dielectric permittivity as a function of doping, shown in Fig. 9b, supports the results obtained from the real part.

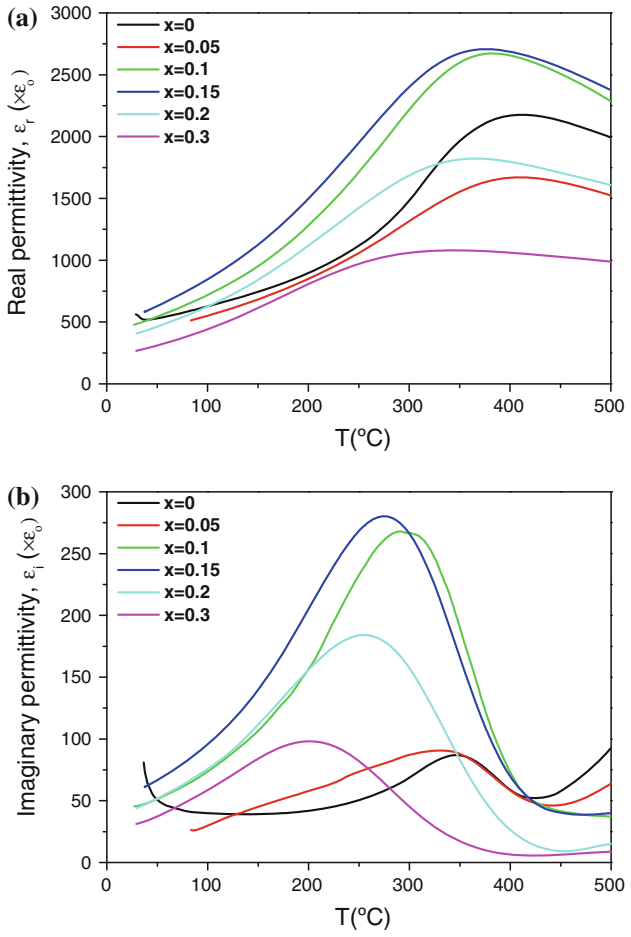

Fig. 9 Temperature dependence of the permittivity on heating: **a** real part, **b** imaginary part, at 1 MHz for the $(1 - x)$ $Bi_{1/2}K_{1/2}TiO_3 - x$ $BiScO_3$ ceramics as a function of composition

It should also be mentioned that the temperature of the permittivity maximum decreases with increasing x from $x = 0$ to $x = 0.3$. Li et al. [17] reported a decrease both in the T_C and T_{O-T} temperatures in the $(1 - x)$ $Na_{1/2}K_{1/2}NbO_3 - x$ $BiScO_3$ ceramics with the addition of bismuth and scandium. More precisely, they determined this downward shift to be a linear decrease, with a diminishing rate of ~38.1 and ~49.9 °C/0.01 mol of BS. Furthermore, they gave full account of the relaxor behavior developed for $x \geq 0.015$. This gradual change from conventional ferroelectric to relaxor ferroelectric with increasing amount of bismuth and scandium content, that in our case happened for $x \geq 0.05$ has also been reported for the $(1 - x)$ $BaTiO_3 - x$ $BiScO_3$ system [9], in which the relaxor behavior is observed for concentrations from 10 to 40 mol% Bi and Sc.

Ferroelectric properties

The ferroelectric hysteresis loops at 0.1 Hz for the $(1 - x)$ $Bi_{1/2}K_{1/2}TiO_3 - x$ $BiScO_3$ ceramics with $x = 0$, 0.05, 0.1, 0.15, 0.2, and 0.3 are shown in Fig. 10. Loops are presented after compensation by subtracting the linear polarization and conduction contributions. Macroscopic ferroelectricity is clearly demonstrated for $x < 0.3$. Unsaturated ferroelectric loops are observed for $Bi_{1/2}K_{1/2}TiO_3$. The coercive field seems to initially increase when 5% of bismuth and scandium are introduced, while clearly decreases with further addition coinciding with the formation of the high temperature relaxor state. Also, a simultaneous decrease of the remnant polarization occurs, typical of an increasing stabilization of this relaxor state at room temperature. The results clearly indicate that a ferroelectric order develops from the relaxor state, yet at an apparently decreasing temperature with increasing x value. This is the same behavior described in the model $(1 - x)$ $Pb(Mg_{1/3}Nb_{2/3})O_3 - x$ $PbTiO_3$ relaxor system with decreasing x [28]. It is also analogous to the effect of Bi and Sc content on the lead-free $(1 - x)$ $Na_{1/2}K_{1/2}NbO_3 - x$ $BiScO_3$ ceramics reported by Li et al. [17]. However, these authors investigated the effect of the introduction of small proportions of these elements. Specifically, the range of compositions studied in that study was $0 \leq x \leq 0.025$. Although they observed saturated loops for all compositions, they also detected a substantial decrease in the E_c with increasing x. Their results accounted for a tetragonal to pseudocubic phase transition occurring at room temperature for $x > 0.02$ together with a gradual transformation from conventional ferroelectric to relaxor ferroelectric starting around $x \sim 0.015$ as that shown for the $(1 - x)$ BKT $- x$ BS in the

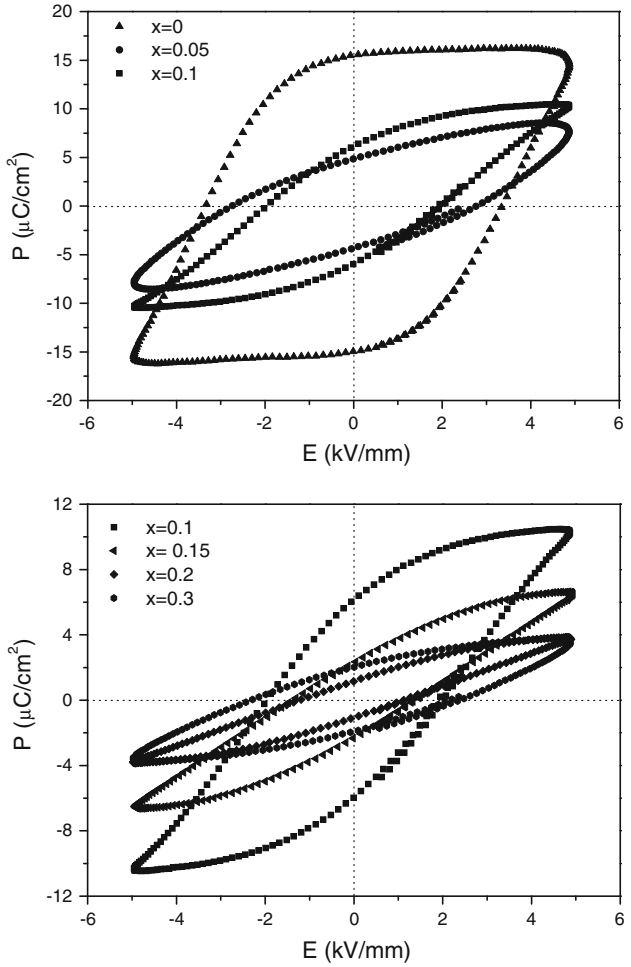

Fig. 10 *P–E* hysteresis loops of the $(1 - x)$ BKT $- x$ BS ceramics: *top* with $x = 0$, 0.05, and 0.1; *bottom* with $x = 0.1$, 0.15, 0.2, and 0.3 under an ac field of 5 kV/mm at room temperature

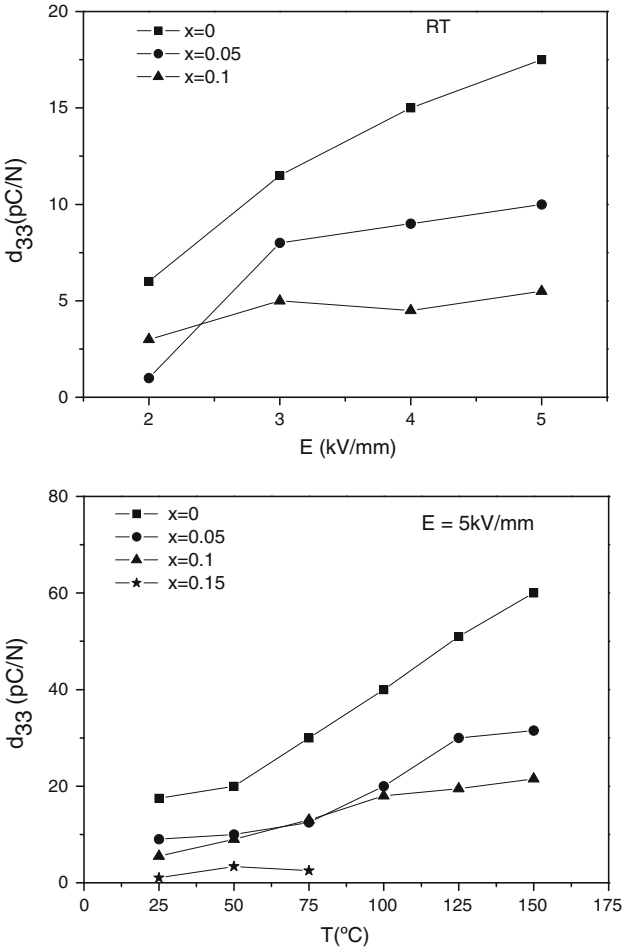

Fig. 11 Piezoelectric coefficient d_{33} as a function of poling field (*top*) and temperature (*bottom*) for the $(1 - x)$ $Bi_{1/2}K_{1/2}TiO_3 - x$ $BiScO_3$ ceramics with $x = 0$, $x = 0.05$, $x = 0.1$, and $x = 0.15$

range $0.05 < x \leq 0.3$. In this latter report, very small doping has a positive effect on the ferroelectric properties, increasing P_r and decreasing E_c, but once the optimum values are reached (25.8 μC/cm^2 for $x = 0.01$) P_r drops with increasing x, as the relaxor state appears, with the E_c diminution continuing, as reported here. This is another example of how the emergence of relaxor states results in the devaluation of the ferroelectric properties.

Piezoelectric properties

On one hand, the poling study indicates that we are far from saturation for the ferroelectric phases under the conditions studied, especially in the case of $Bi_{1/2}K_{1/2}TiO_3$, whose piezoelectric coefficient d_{33} increases almost linearly with the poling field in the range investigated (Fig. 11), as well as with temperature up to 150 °C. Dielectric breakdown prevented poling at higher fields and/or higher temperatures. It is reported in the literature that the high conductivity of BKT bulk ceramics typically causes difficulties in poling and a significant deterioration in polarization properties [29]. On the other hand, saturation is reached for relaxor phases, $(x \geq 0.1)$, though with lower values of piezoelectric coefficient than for BKT under the same conditions.

Note that a maximum d_{33} of 60 pC/N has been achieved for BKT in this study, and even lower values were obtained for the $Bi_{1/2}K_{1/2}TiO_3$–$BiScO_3$ solid solution. This is far from values reported for $BiScO_3$–$PbTiO_3$ at the MPB (450 pC/N). Nevertheless, BKT is a tetragonal perovskite, and high piezoelectric activity is not expected. Also, a relaxor state rather than a MPB result of BS addition, so high piezoelectric coefficients could not be expected either.

In summary, results clearly indicate that a ferroelectric MPB with high piezoelectric coefficient does not occur in the $(1 - x)$ $Bi_{1/2}K_{1/2}TiO_3 - x$ $BiScO_3$ system. Instead, a relaxor state develops between $x = 0.05$ and 0.1. Relaxor ferroelectrics are a special type of polar materials characterized by compositional disorder in one (or more) lattice

sites and short-range polar order [27]. This consists in polar nanoregions (PNRs) embedded in a non-polar matrix, whose dynamics are responsible of their distinctive dielectric properties [30]. PNRs are thought to nucleate around chemically ordered regions (CORs) [31], which have been observed in a number of model relaxors as $Pb(Mg_{1/3}Nb_{2/3})O_3$, and have been proposed to result of the inability of the system to attain the ordered ground state because of kinetic issues [30]. Short-range A-site ordering has been described in lead-free $Bi_{1/2}Na_{1/2}TiO_3$ [32], and an analogous tendency might be assumed for $Bi_{1/2}K_{1/2}TiO_3$. If this were the case, results here reported would suggest $BiScO_3$ addition to promote the formation of CORs, and so of a relaxor state, yet determination of the specific mechanism requires further research. This is in contrast with the behavior described in $BiScO_3$–$PbTiO_3$, for which a MPB is indeed formed, and strongly indicates that tendency to A-site ordering might be an important aspect to be taken into account when designing novel free MPB systems.

Conclusions

Single phase $(1-x)\ Bi_{1/2}K_{1/2}TiO_3 - x\ BiScO_3$ perovskite-type solid solutions can be synthesized via a solid-state reaction method up to $x = 0.2$. In the case of $Bi_{1/2}K_{1/2}TiO_3$, synthesis was achieved at 960 °C, which is a significantly lower temperature than those previously reported.

Furthermore, dense ceramics can be obtained at temperatures ≤1000 °C for all the compositions under study, by conventional sintering. In the case of $Bi_{1/2}K_{1/2}TiO_3$, sintering was achieved at only 960 °C, which again is a significantly lower temperature than those previously reported.

The crystalline structure evolves from tetragonal for $x < 0.1$ to pseudocubic for $0.1 \leq x \leq 0.3$ and a simultaneous change in the electrical and electromechanical properties is observed. The main result is a clear transition from conventional ferroelectric for compositions with $0 \leq x \leq 0.05$ to a relaxor ferroelectric behavior for those with $0.1 \leq x \leq 0.3$. This contradicts previous reports of relaxor behavior of $Bi_{1/2}K_{1/2}TiO_3$, and suggests a main role of the specific defect chemistry resulting of the synthesis and sintering. Good ferroelectric and piezoelectric properties are found for the conventional ferroelectric compositions ($0 \leq x \leq 0.05$), though their high values of the coercive field hindered the attainment of the saturation of polarization.

Acknowledgements L. M acknowledges the financial support of the Spanish Consejo Superior de Investigaciones Científicas (CSIC, JAEPre086). This research has been funded by Ministerio de Ciencia e Innovación (MICINN, Spain) through the MAT2010-18543 project. The authors are also grateful for the technical support provided by Mrs I. Martínez.

References

1. Shrout TR, Zhang SJ (2007) J Electroceram 19:113. doi:10.1007/s10832-007-9047-0
2. Guo R, Cross LE, Park SE, Noheda B, Cox DE, Shirane G (2000) Phys Rev Lett 84:5423. doi:10.1103/PhysRevLett.84.5423
3. Zhou CR, Liu XY, Li WZ, Yuan CL (2009) J Phys Chem Solid 70:541. doi:10.1016/j.jpcs.2008.12.013
4. Yang ZP, Liu B, Wei LL, Hou YT (2008) Mater Res Bull 43:81. doi:10.1016/j.materresbull.2007.02.016
5. Takenaka T, Nagata H (2005) J Eur Ceram Soc 25:2693. doi:10.1016/j.jeurceramsoc.2005.03.125
6. Zhou CR, Liu XY, Li WZ, Yuan CL (2009) Solid State Commun 149:481. doi:10.1016/j.ssc.2008.12.034
7. Saito Y, Takao H, Tani T, Nonoyama T, Takatori K, Homma T, Nagaya T, Nakamura M (2004) Nature 432:84. doi:10.1038/nature03028
8. Tinberg DS, Trolier-Mckinstry S (2007) J Appl Phys 101:024112. doi:10.1063/1.2430627
9. Ogihara H, Randall CA, Trolier-Mckinstry S (2009) J Am Ceram Soc 92:110. doi:10.1111/j.1551-2916.2008.02798.x
10. Takenaka T, Maruyama K, Sakata K (1991) Jpn J Appl Phys 30:2236. doi:10.1143/JJAP.30.2236
11. Eitel RE, Randall CA, Shrout TR, Park SE (2002) Jpn J Appl Phys 41:2099. doi:10.1143/JJAP.41.2099
12. Zhang SJ, Randall CA, Shrout TR (2003) Appl Phys Lett 83:3150. doi:10.1063/1.1619207
13. Eitel RE, Randall CA, Shrout TR, Rehrig PW, Hackenberger W, Park SE (2001) Jpn J Appl Phys 40:5999. doi:10.1143/JJAP.40.5999
14. Chaigneau J, Kiat JM, Malibert C, Bogicevic C (2007) Phys Rev B 76:094111. doi:10.1103/PhysRevB.76.094111
15. Hungría T, Houdellier F, Algueró M, Castro A (2010) Phys Rev B 81:100102(R). doi:10.1103/PhysRevB.81.100102
16. Rodel J, Jo W, Seifert KTP, Anton EM, Granzow TK, Damjanovic D (2009) J Am Ceram Soc 92:1153. doi:10.1111/j.1551-2916.2009.03061.x
17. Li XH, Jiang M, Liu J, Zhu JL, Zhu XH, Li LH, Zhou Y, Zhu JG, Xiao DQ (2009) Phys Status Solidi A 206:2622. doi:10.1002/pssa.200925036
18. Datta K, Thomas PA (2010) J Appl Phys 107:043516. doi:10.1063/1.3309064
19. Zhong W, Vanderbilt D (1994) Phys Rev Lett 73:1861. doi:10.1103/PhysRevLett.73.1861
20. Hiruma Y, Aoyagi R, Nagata H, Takenaka T (2005) Jpn J Appl Phys 44:5040. doi:10.1143/JJAP.44.5040
21. Zhao SC, Li GR, Ding AL, Wang TB, Yin QR (2006) J Phys D 39:2277. doi:10.1088/0022-3727/39/10/042
22. Hou YD, Hou L, Huang SY, Zhu MK, Wang H, Yan H (2006) Solid State Commun 137:658. doi:10.1016/j.ssc.2006.01.023
23. Li ZF, Wang CL, Zhong WL, Li JC, Zhao ML (2003) J Appl Phys 94:2548. doi:10.1063/1.1592290
24. Hou L, Hou YD, Song XM, Zhu MK, Wang H, Yan H (2006) Mater Res Bull 41:1330. doi:10.1016/j.materresbull.2005.12.010
25. Wada T, Toyoike K, Imanaka Y, Matsuo Y (2001) Jpn J Appl Phys 40:5703. doi:10.1143/JJAP.40.5703
26. Yang JF, Hou YD, Wang C, Zhu MK, Yan H (2007) Appl Phys Lett 91:023118. doi:10.1063/1.2754366
27. Cross LE (1987) Ferroelectrics 76:241

28. Jiménez R, Jiménez B, Carreaud J, Kiat JM, Dkhil B, Holc J, Kosec M, Algueró M (2006) Phys Rev B 74:184106. doi:10.1103/PhysRevB.74.184106
29. Hiruma Y, Marumo K, Aoyagi R, Nagata H, Takenana T (2008) J Electroceram 21:296. doi:10.1007/s10832-007-9146-y
30. Bokov AA, Ye ZG (2006) J Mater Sci 41:31. doi:10.1007/s10853-005-5915-7
31. Burton BP, Cockayne E, Waghmare UV (2005) Phys Rev B 72:064113. doi:10.1103/PhysRevB.72.064113
32. Trolliard G, Dorcet V (2008) Chem Mater 20:5074. doi:10.1021/cm800464d